Arabian Journal of Chemistry (2022) **15**, 103520

King Saud University

Arabian Journal of Chemistry

www.ksu.edu.sa
www.sciencedirect.com

ORIGINAL ARTICLE

Modified silicon carbide NPs reinforced nanocomposite hydrogels based on alginate-gelatin by with high mechanical properties for tissue engineering

Mojgan Ghanbari [a], **Masoud Salavati-Niasari** [a,*], **Fatemeh Mohandes** [a], **Zohreh Firouzi** [b]

[a] *Institute of Nano Science and Nano Technology, University of Kashan, Kashan, P.O. Box. 87317–51167, Iran*
[b] *Department of Pharmaceutical Nanotechnology, School of Pharmacy, Mashhad University of Medical Sciences, Mashhad, Iran*

Received 30 July 2021; accepted 21 October 2021
Available online 27 October 2021

KEYWORDS

Tissue Engineering;
Inorganic reinforcement;
Silicon Carbide;
Injectable hydrogel;
Rheological properties;
Alginate-Gelatin Nanocomposites

Abstract Hydrogels are encouraging for different clinical purposes because of their high water absorption and mechanical relation to native tissues. Injectable hydrogels can modify the invasiveness of utilization, which decreases recovery and surgical costs. Principal designs applied to create injectable hydrogels incorporate in situ formation owing to chemical or/and physical crosslinking. Here, we report nontoxic, thermosensitive, injectable hydrogels composed of gelatin (GEL) and oxidized alginate (OA) reinforced by silicon carbide nanoparticles (SiC NPs) and crosslinked with N-hydroxysuccinimide (NHS) and 1-ethyl-3-(3-dimethylaminopropyl) carbodiimide (EDC). The mechanical characteristics of the hydrogels were examined via rheological analysis. The outcomes reveal that extending the SiC NPs contents enhances the mechanical properties around five times. The cross-sectional microstructure of the scaffolds comprising 0.25, 1.0, and 1.5% SiC NPs was scrutinized by FESEM, verifying porous structure with interconnected pores. Because of the smaller pore sizes in the hydrogels, the swelling rate has reduced at the higher content of SiC, which diminishes the water uptake. Additionally, the biodegradation study unveils that the hydrogels with SiC are more long-lasting than the hydrogel without SiC. By adding SiC NPs, a decrease is observed in the biodegradation and swelling ratio. The scaffold with a higher SiC NPs content (1.5%) mani-

* Corresponding author.
E-mail address: salavati@kashanu.ac.ir (M. Salavati-Niasari).
Peer review under responsibility of King Saud University.

Production and hosting by Elsevier

https://doi.org/10.1016/j.arabjc.2021.103520

fested better cell attachment and was less cytotoxic than hydrogel without SiC. OA/GEL composites embedded SiC NPs have manifested excellent physical properties for tissue engineering in comparison with hydrogel without nanoparticles.

1. Introduction

Articular cartilage is a well-organized tissue with significant flexibility. Nevertheless, it has restricted intrinsic healing capability upon changes caused by diseases, aging, and trauma (Vinatier & Guicheux, 2016). The control of articular cartilage injuries is one of the top demanding clinical barriers for orthopedic surgeons (Camarero-Espinosa et al., 2016; Morouço et al., 2019). Tissue engineering (TE) intends to improve biological alternatives that can replace the duties of modified tissues (Y. Xu et al., 2019). Cartilage tissue engineering has considerably profited from recent approaches in their interplays in tissue reformation, stem cells and material engineering (Ikada, 2006). In these circumstances, stem cells are frequently seeded within a matrix or onto a scaffold, whose main purpose is to support chondrogenesis and reproduce some of the properties of the target-tissue extracellular matrix (ECM) (Vinatier et al., 2009). Hydrogels have drawn great consideration for regenerative medicine and utilization in TE due to their swelling ability, three dimensional (3D) ECM-mimicking polymeric network, and porous structure, providing for cell embedding (Ahmed, 2015; Hunt et al., 2014). Schiff's base formation (between amine and carbonyl groups to form imines) can be used as a crosslinking technique (Nezhad-Mokhtari et al., 2019; J. Xu et al., 2019). Furthermore, as the hydrogels are temporary scaffolds that mimic ECM, hence the selection of the appropriate biological materials is crucial to provide these hydrogels. Between various polymers, natural polymers, for instance, pectin (Chen et al., 2017), alginate (AL) (Park et al., 2017), gelatin (GEL) (Han et al., 2017), hyaluronic acid (Bian et al., 2011), and chitosan (Jin et al., 2009), are being examined owing to their likeness to the ECM. Alginate is a renowned polysaccharide with a negative charge, which is comprised of 1,4-linked -d-mannuronate (M blocks) and 1,4-linked -l-guluronate (G-blocks) deposits in changeable ratios (Boontheekul et al., 2005). Alginate hydrogels have been utilized as model extracellular matrixes, as scaffolds for tissue engineering, and as delivery vehicles for drugs for fundamental physiological investigations (Tan et al., 2010; Tønnesen & Karlsen, 2002). Besides, the cells cannot easily interact by alginates due to the lack of cell-surface receptors, which provide bonding to alginates as well as prevent protein adsorption in alginate (Boontheekul et al., 2005). Therefore, AL chains were chemically adjusted to display cell-adhesive ligands (Alsberg et al., 2002; Kreeger et al., 2003) or developed to provide well-controlled degradation (Li et al., 2010; Yang et al., 2011).

Moreover, GEL, a natural polymer obtained of the denaturalization of collagens, possesses some unique properties of collagens (Xing et al., 2014), confirming bioactive uses, including cell proliferation and adhesion and also mechanical characteristics. It has been converted into various shapes for biomedical treatments, including scaffolds, particles, hydrogels, and films for tissue engineering dependent on its procedure (Bang et al., 2018). As specific illustrations, GEL was transformed to thermo-reversible hydrogel with a gelation temperature at about 30 °C, subsequently indicating the probability of its utilization in a gel form at body temperature (Kimura et al., 2003; Van Vlierberghe et al., 2011). Porous GEL hydrogels formed by ice particulates and freeze-drying were employed to investigate cells interaction, wherever cells adhesion, distribution, and proliferation was developed by checking their features, including mechanical properties and pore sizes (Chen et al., 2016).

Regardless of the mentioned advantages, GEL and AL have confined mechanical properties and degradation rates, restricting their medical applications. On the other hand, the injectable hydrogels need to supply enough mechanical conditions to promote cell proliferation, migration, and differentiation to regenerate damaged tissue.

Several semiconductors for biotechnical usage have been studied for sensing potentiality and biocompatibility. The principal anxiety is to obtain a desirable substance that creates low or no negative impact when transplanted in the body that can be embedded as long as possible (Bonaventura et al., 2019). Silicon carbide (SiC) has been around for over a century as a manufacturing substance and has exposed broad and diverse applications due to its distinctive thermal and electrical properties. Recently, attention to SiC as a suitable material has been increased for medical applications. It has been confirmed that SiC is a suitable substrate for this aim, being hemo- and biocompatible, and functional for implantable materials fabrication (Oliveros et al., 2013; Saddow, 2012). Before, the principal disadvantages of SiC were the low quality of the substrate (associated with Si) and the high cost. However, material quality has reached very high standards, and the cost has significantly reduced in recent years. Hence implantable radiofrequency (RF) devices have already been manufactured for real-time and in vivo measurements of the glucose and neuronal interface devices (Afroz et al., 2013; Frewin et al., 2014). Therefore, SiC is considered a proper bridge among external electronic devices and internal neural networks (Frewin et al., 2014). This is the first effort that silicon carbide nanoparticles (SiC NPs) are applied as support to fabricate nanocomposite hydrogels with enhanced mechanical properties.

In the current study, we fabricated injectable hydrogels based on the Schiff's base reaction, formed of oxidized alginate (OA), and gelatin (GEL) reinforced with different contents of SiC NPs. The physicochemical properties of hydrogels, including swelling ratio, biodegradation, mechanical properties, and pore sizes were affected by changing the weight ratios of SiC NPs. Cell proliferation and in vitro biodegradability were investigated using fibroblast cell lines (L929 cells) embedded into the scaffolds.

2. Experimental

2.1. Materials

Sodium alginate (low viscosity derived from brown algae), Gelatin (type B from bovine skin), acetone, potassium periodate (KIO_4), silver nitrate ($AgNO_3$), ethyl alcohol, n-propanol, 1-ethyl-3-(3-dimethylaminopropyl) carbodiimide (EDC), ethylene glycol, sodium chloride, N-hydroxysuccinimide (NHS) were acquired from Merck and Sigma-Aldrich Company and employed without additional refinement. Silicon Carbide Nanopowder/Nanoparticles (SiC, beta, 99 + %, < 80 nm, cubic) were purchased from US Research Nanomaterials, Inc.

2.2. Alginate oxidation

2.01 g of sodium alginate and 11.2 ml of n-propanol were blended with DI-water in a 250-mL beaker to obtain 225 ml in total. The mix was kept at 30 °C in the dark under stirring (5 h) to dissolve alginate completely. 1.16 g of Potassium periodate (KIO_4) dispersed in 30 ml DI-water was combined with alginate solution. The mixture was kept in the dark for 24 h. The reaction was quenched by adding 1 ml of Ethylene glycol

(EG), and the mix was agitated for another 30 min. 6.5 g of Sodium chloride (NaCl) was dissolved in the above suspension to purify the polymer, which was next gently added to 400 ml agitated ethyl alcohol. The white precipitate was dissolved in DI-water with 3.3 g of NaCl and reprecipitated in 250 ml ethyl alcohol. The precipitate was dissolved in DI-water again and precipitated in 200 ml acetone. Eventually, the precipitate was rinsed in agitated ethyl alcohol for 15 min, refined, and dried at 25 °C (Rogalsky et al., 2011). The lack of periodate was controlled by combining 500 μL fractional of the dialyzate to 500 μL of a 1% silver nitrate solution, and assuring the nonexistence of any precipitate (Balakrishnan & Jayakrishnan, 2005).

2.3. OA/GEL/SiC scaffolds formation

4 ml of 6 wt% of OA solution was agitated with 4 ml of 15 wt % of GEL at 37 °C. The cross-linker, including a mixture of 0.1 g EDC and 0.05 g NHS, was added to the above solution. The first gelation was observed in 4–5 s and kept at 37° C, resulting in the creation of a perfect gel after 2 min. Different weight percentages of SiC (0.25%, 1.0%, and 1.5%) was added to the 4 ml of 6 wt% of OA solution and agitated for 5 min. Next, 4 ml of 15 wt% of GEL was added to the suspension and stirred for another 5 min. The final solutions were mixed for 2 min by adding EDC and NHS as cross-linker agents. The samples were freeze-dried for 24 h. Three-dimensional scaffolds with a diameter of about 2 cm and a thickness of 1 cm were produced.

2.4. Swelling behavior and in vitro biodegradation

The water absorption of hydrogels was evaluated by the gravimetric technique. About 0.2 g (M_0) of the hydrogels were incubated in 10 ml PBS for 24 h to attain equilibrium swelling. The buoyant was removed and the swollen hydrogel were weighed (M_s). The swelling ratio (SR) was expressed by the following equation (Nguyen & Lee, 2011):

$$SR(\%) = \frac{M_s - M_O}{M_O} \times 100 \quad (1)$$

Mass degradation/erosion degrees were additionally evaluated likewise at various periods up to 21 days. All tests were accomplished five times.

2.5. Materials characterizations

Fourier transform infrared spectroscopy (Shimadzu Varian 4300 spectrophotometer) was utilized to investigate the chemical composition of oxidized alginate and the fabricated hydrogels applying KBr pellets in the wavenumber between 4000 and 400 cm^{-1}. A field emission scanning electron microscopy (TESCAN MIRA 3 FE-SEM) was used to study the morphological and structural of lyophilized hydrogels. The lyophilized hydrogels were cross-sectioned, coated by gold (Au), and detected by FE-SEM at an accelerating voltage of 15 kV. High-resolution transmission electron microscopy (EM 208, Philips HR-TEM with an accelerating voltage of 100 kV) was utilized to observe carbon nitride quantum dots. A Physica MCR 300 Rheometer (Anton Paar Ltd., Austria) was utilized to measure the oscillatory rheological properties of the hydrogels.

2.6. Mechanical features

A Physica MCR 300 Rheometer (Anton Paar Ltd., Austria) was used to measure the rheological attributes of the hydrogels utilizing a circular disk parallel plate with a diameter of 25 mm and a gap of 0.5 mm. An amplitude sweep was conducted at a consistent angular frequency of 1 Hz to define the limit of linear viscoelasticity. The strain amplitude was kept at 0.1% during the test. The contribution of the liquid-like form (viscous modulus (G‘‘)) and solid-like form (elastic modulus (G’)) were noted through temperature sweep from 20 to 50 °C at a speed of 1 °C min^{-1} to assess thermogelling attributes (angular frequency = 1 Hz). Each following rheological test was conducted below simulated physiological states (in PBS pH = 7.4 at 37 °C), considering the possible utilization of hydrogels. The oscillatory rheological determination as a function of time was conducted at a consistent frequency of 1 Hz to evaluate the time of gelation. The gel point or gelation time was specified as the time that the loss modulus and shear storage modulus were identical (Macaya et al., 2011). The hydrogels were swollen for 1 h in 1 ml PBS and moved to the rheometer stage for performing crosslinked hydrogels. Next, frequency sweep analyses in the linear viscoelastic area were performed to determine the dynamic viscoelasticity at 37 °C on a broad range of frequencies (0.1–100 Hz).

2.7. In vitro biological assays

The cytotoxicity of scaffolds with and without SiC NPs was evaluated utilizing the methyl thiazolyl tetrazolium (MTT) assay. In brief, L929 cells with a density of 5×10^3 cells/mL were seeded in 96-well microplates in complete Roswell Park Memorial Institute media (RPMI) comprising 1% penicillin–streptomycin and 10% heat-inactivated fetal bovine serum (FBS). The plates were incubated with 5% CO_2 in a 95% humidified atmosphere at 37 °C for 48 h. Scaffolds were immersed in 70% ethanol for 1 h, rinsed five times with cold sterile phosphate-buffered saline (PBS), and added into the medium with successive concentrations (20, 50, and 100 μg/mL), and cultured for 24 and 72 h. After incubation time the supernatants were trashed, 100 μL in complete RPMI media comprising 10% MTT stock solution were added per wells. Cells were incubated at 37 °C for 4 h again. The medium was discharged and the reaction was terminated by adding 100 μL dimethyl sulfoxide (DMSO) per wells to solubilize formed formazan crystals. Finally, the optical densities were measured by a microplate reader (Microplate Reader Gmi. Ltd., USA, Awareness Technology Stat Fax 2100) at 570 nm with background subtraction at 630 nm after 1 h. The cell viability percentage was assessed for the control.

To study the morphology of the cells attached to the scaffolds, the scaffolds were soaked in 70% ethanol for 1 h and rinsed five times with sterilized PBS. Sterilized scaffolds were placed in 6-well cell culture plates (Corning-Costar, Corning, NY). Cells were seeded with 5 ml cell suspension comprising 5×10^3 cells/ml on scaffolds for 24 h. Scaffolds were monitored by Phase-contrast microscope (Olympus America, Inc). Cell-seeded scaffolds were picked up from the media and fixed

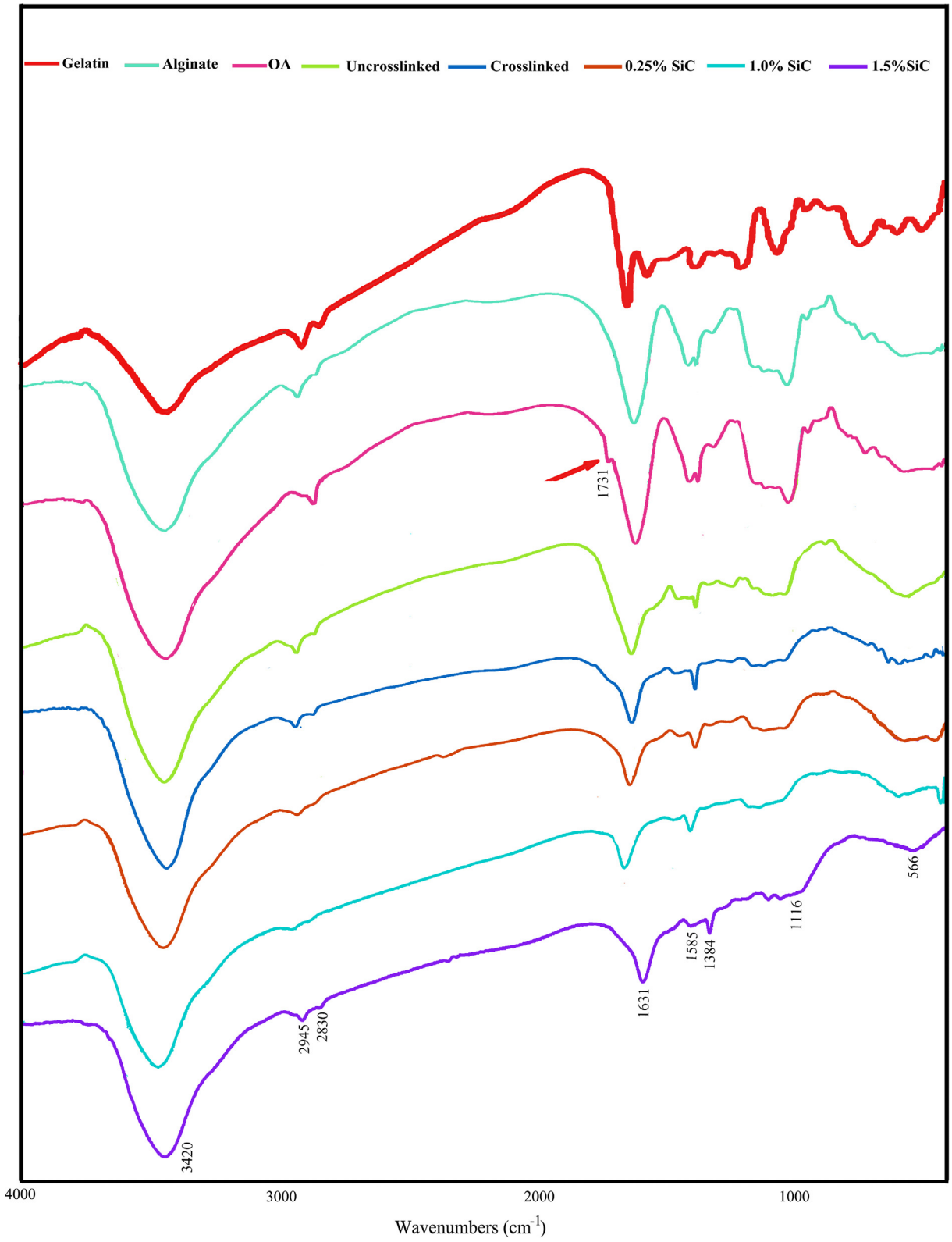

Fig. 1 FTIR spectrum of gelatin, alginate, oxidized alginate, and the hydrogels.

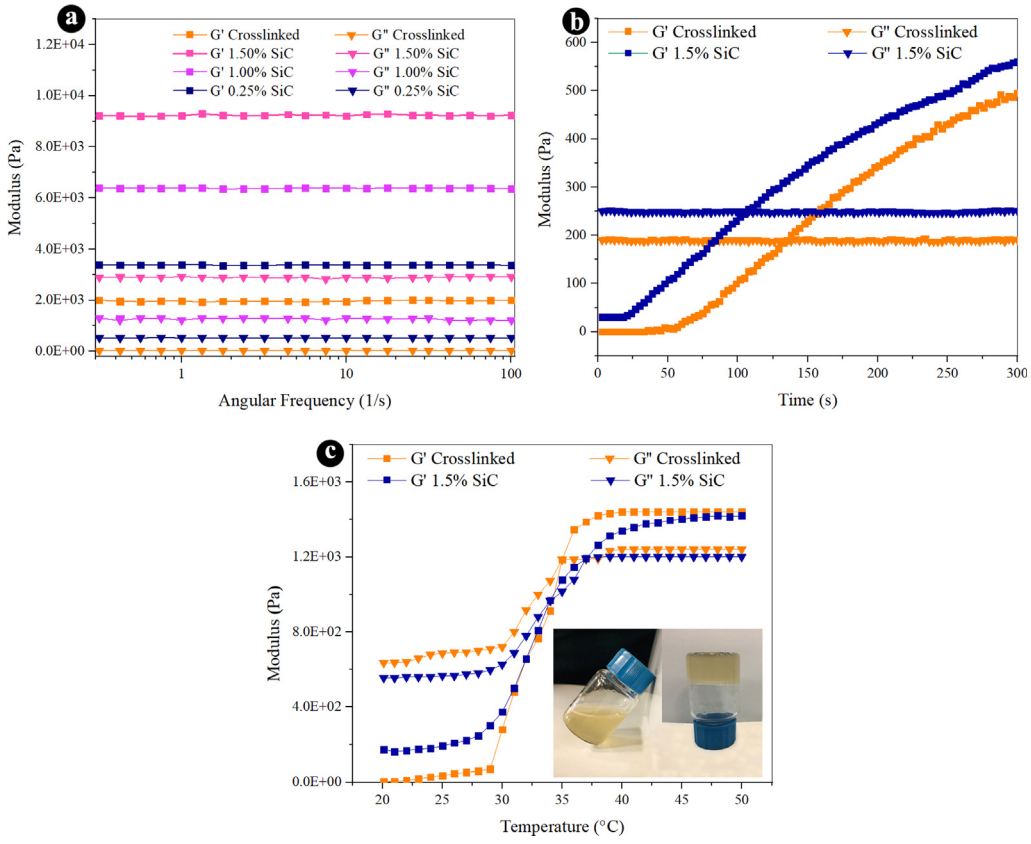

Fig. 2 Rheological properties of the hydrogels by (a) frequency sweep, (b) time sweep, and (c) temperature sweep.

Table 1 Rheological properties of the hydrogels at 37 °C and frequency of 1 Hz.

Sample	Storage modulus (Pa)	Loss modulus (Pa)	Pore size (μm)
Crosslinked	1962 ± 42	24.6 ± 1.6	235.0 ± 139
0.25% SiC	3370 ± 20	525 ± 2	200.0 ± 126
1.0% SiC	6370 ± 20	1247 ± 47	194.9 ± 119
1.5% SiC	9247 ± 47	2870 ± 49	146.5 ± 88

with glutaraldehyde as fixator. In summary, scaffolds were gently rinsed with PBS (pH = 7.4) three times then soaked in 2.5% glutaraldehyde solution at 4 °C for 12 h. The fixative was discharged and was dehydrated carefully with ethanol at a series of concentrations and placed for drying overnight in a desiccator. The morphology of the scaffold surface was studied by scanning electron microscopy (SEM, MIRA3-TESCAN).

3. Result and discussion

3.1. FTIR spectra of hydrogels

The architectural variations in gelatin, alginate, OA, and fabricated hydrogels were studied by FTIR spectroscopy (Fig. 1). The FTIR spectrum of gelatin shows that the region of 3000–3600 cm^{-1} and 1100–1700 cm^{-1} contains the most potentially useful information bearing on the structure of gelatin. The band identified as N—H stretching vibrations are considered to be hydrogen bonded. The frequency N—H band was observed at 3431 cm^{-1} that is a characteristic of N—H stretching of secondary amide II bands. The spectrum of gelatin also shows the peaks at 1631 and 1639 cm^{-1} due to C═O stretching (amide I bands). The characteristic bands at 1550 cm^{-1} and 1500 cm^{-1} corresponded to N—H bending and amide II bands (Pawde & Deshmukh, 2008). N—H out of plane wagging is located at 670 cm^{-1}. The peaks at 2922 cm^{-1} and 2850 cm^{-1} are related to C—H stretching (Tengroth et al., 2005). The band at 1240 cm^{-1} presented amide III. The amide I band predominantly arises from the protein amide C═O stretching vibration, and amide II absorption is caused by N—H bending and C—N stretching vibrations, and the amide III peak is made up of C—N stretching vibration (Baniasadi et al., 2016). Fig. 1 shows some changes in characteristic bands of alginate spectrum after the oxidation, equivalent to reported literature (Jejurikar et al., 2012; Sarker et al., 2014). As displayed in the OA spectrum, the specific absorption bands correlated to AL structure lightly change, and a unique band arrives at 1731 cm^{-1} assigned to the aldehyde group. The absorption bands at 1384 cm^{-1} and 1631 cm^{-1} are also existing in OA, which are assigned to symmetric and asymmetric —COO— stretching vibrations on the AL structure, respectively (Emami et al., 2018). The peaks at around 3000 cm^{-1} are attributed to asymmetric (2945 cm^{-1}) and symmetric (2850 cm^{-1}) stretching modes of —CH_2 groups (Kuzmanović et al., 2017). Hence, the oxidation reaction via potassium periodate did not influence the carboxyl groups in AL. The new

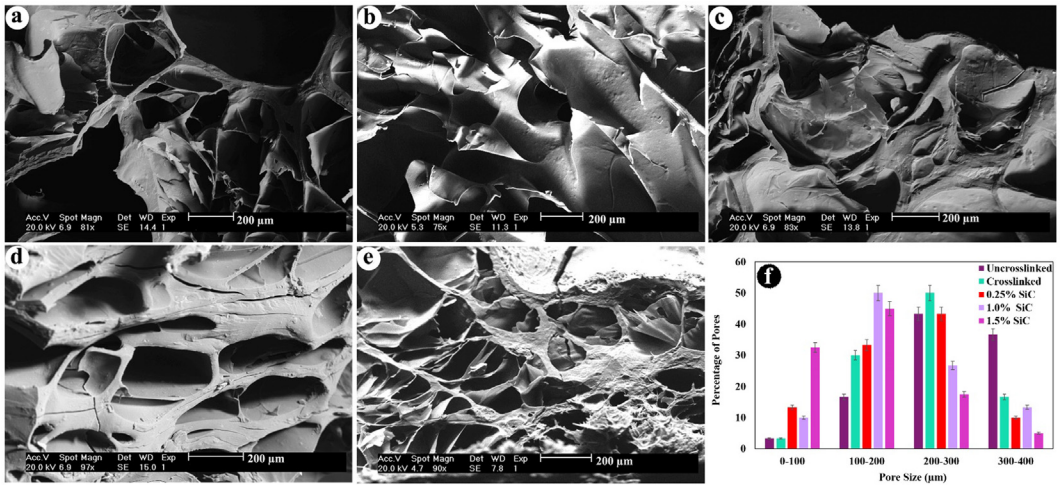

Fig. 3 Cross-section morphology of freeze dried hydrogels (a) uncrosslinked, (b) crosslinked, (c) containing 0.25% SiC, (d) 1.0% SiC, (e) 1.5% SiC, and (f) size distribution diagram of the samples.

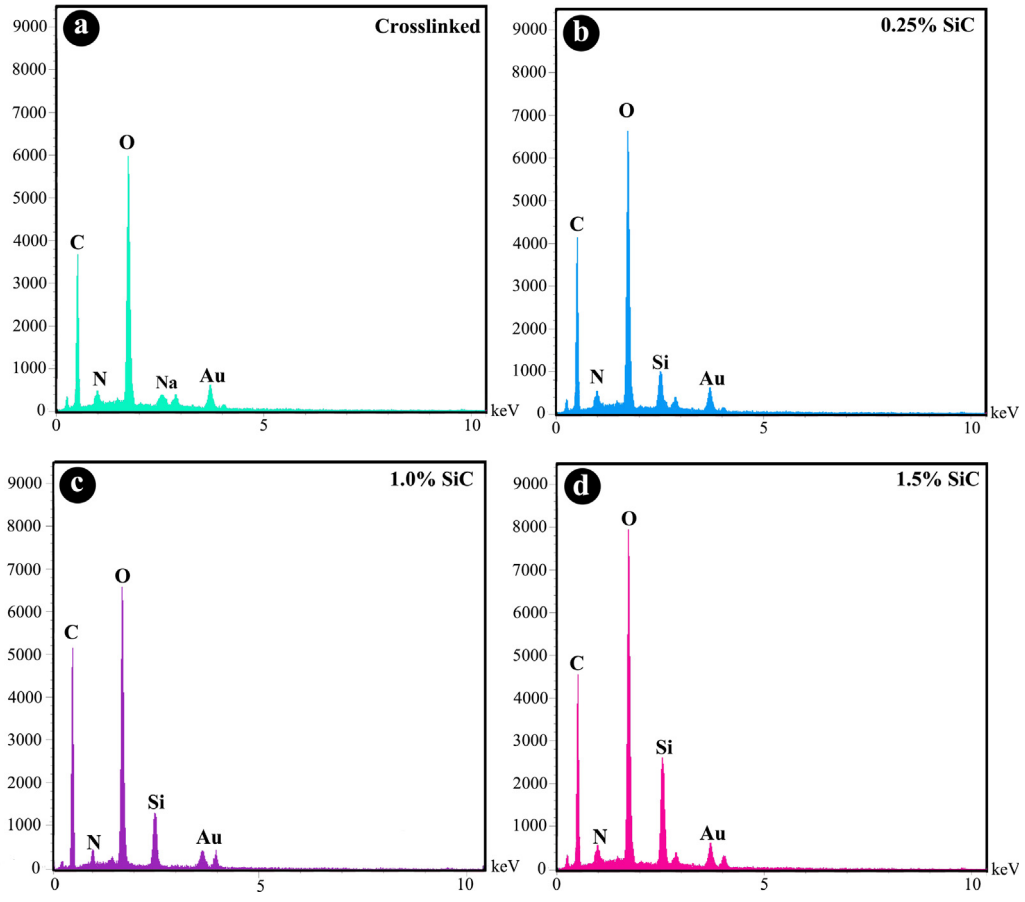

Fig. 4 EDS spectra of freeze dried hydrogels (a) crosslinked, (b) containing 0.25% SiC, (c) 1.0% SiC, and (d) 1.5% SiC.

peak at 1731 cm^{-1} in the OA shows the appearance of aldehyde groups (—CHO). In some circumstances, this band is not recognized because of the hemiacetal configuration of hydroxyl groups with free aldehydes groups on the neighboring D-glucuronic acid subunits (Jejurikar et al., 2012; Vieira et al., 2008). The broad characteristic band at 3420 cm^{-1} is associated with the —OH stretching vibration. The stretching vibration of the H-C aldehyde can be seen around 2830 cm^{-1} (Bock & Gierlinger, 2019). The characteristic peaks at 1631 and 1384 cm^{-1} indicate the vibration of C=N of gelatin, showing the production of Schiff's base. As displayed in Fig. 1, a small shift is visible in the characteristic peak of OA in the spectrum of OA-GEL cross-linked hydrogel. Furthermore, the aldehyde group band of OA at 1731 cm^{-1}

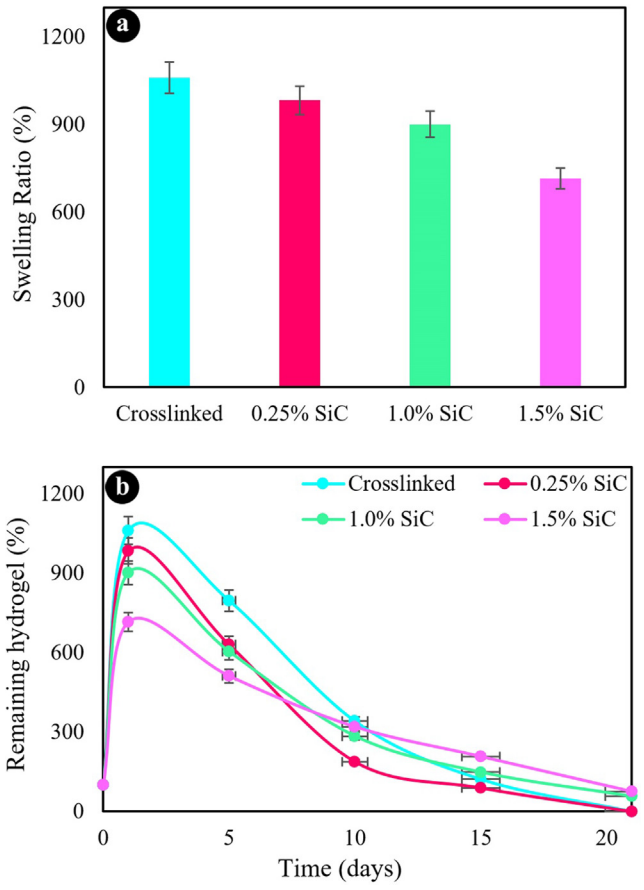

Fig. 5 (a) Swelling ratio of the hydrogels, (b) in vitro biodegradation after various incubation times in PBS at 37 °C.

has vanished, and a new band emerged at 1585 cm^{-1} assigned to CN double bond (Baniasadi et al., 2016). The new band is because of the Schiff-Base reaction within the amine group of gelatin and the aldehyde group of OA (Sarker et al., 2014), which proved that the cross-linking of OA and GEL occurred. Absorption peak at 566 cm^{-1} corresponded to the stretching vibration of Si—C bond. The addition of SiC NPs did not change the FTIR spectra of the hydrogels due to the low amounts of SiC in the hydrogel network.

3.2. Mechanical properties

Viscoelastic behavior of the injectable hydrogels was assessed utilizing frequency sweep tests to evaluate the dynamic storage modulus (G') and the loss modulus (G''), which are presented in Fig. 2a. Likewise, G' is much higher than G" in all hydrogels, showing that the samples are very elastic. By raising the SiC contents, the magnitude of the moduli is significantly higher, increasing by around 5 orders of magnitude associated with the hydrogel without SiC (Table 1 and Fig. 3a). Increasing the SiC contents can drive to a higher physical crosslinking formation as it promotes mechanical behavior and gel formation within the presence of different reactive elements.

Another essential aspect of injectable hydrogel design is the gelation time. The hydrogel formation should be gradually enough so that biomolecules and cells can be incorporated uniformly inside them, and they must remain liquid during surgery and injections. Nevertheless, after injection, they should immediately transform into the gel, therefore, that they cannot abandon the injection part (Epstein-Barash et al., 2012). The time sweep of the crosslinked hydrogel and hydrogel containing 1.5% SiC was performed to check the time of gelation at human body temperature (37 °C). Before gelation, the G'' is higher than the G', which means a liquid form, and the predominant viscoelasticity during the gelation is begun. G' grows quicker than G" by progressing the time, suggesting transition into a solid-like phase with great elasticity (Fig. 2b). The gelation time of crosslinked hydrogel is 135 s, which is sufficient for acting as an injectable hydrogel. The gelation time of hydrogel has decreased to 100 s by adding SiC NPs due to the formation of physical crosslinking of SiC with the hydrogel network. In clinical treatments, quick gelation is aspired to restrict the diffusion of bioactive molecules/cells or hydrogel precursors to the surrounding tissue (Chiu et al., 2009; Choi et al., 2003; Hiemstra et al., 2007).

The temperature sweep analysis was utilized to study the thermoresponsive behavior of the crosslinked hydrogel and hydrogel containing 1.5% SiC. The temperature was boosted from 20 to 50 °C at a rate of 1 °C min^{-1} (Fig. 2c). G' was lower than G'' at lower temperatures, signifying a liquid-like form. G' grown prominently faster than G" throughout the heating procedure. At greater temperatures, G' enhanced greatly larger than G'', indicating a gel-like form. The G' and G" are nearly parallel straight lines under the gelation temperature, and the amount of G' is more than G'' after the sol/gel transformation. When the temperature is above the gel point, the elastic modulus is greater than the viscous modulus recommending transformation into the solid state. The crossing point of G' and G" is the temperature of gelation (35 °C) and is usually indicated as the sol/gel conversion temperature (Li et al., 2015). The addition of silicon carbide nanoparticles has brought the gelation temperature closer to body temperature (37 °C). The gelation temperature of the hydrogel containing 1.5% SiC was obtained at 37 °C.

3.3. Structure of hydrogels

As one of the main features for cartilage tissue engineering, hydrogels must possess extremely porous and interconnected pore composition to assure a suitable biological environment for cell proliferation, cell attachment, and supplying the nutrient flow passage (Zhu et al., 2009). The pore size and morphological structure depend on the content and molecular mass of the polymer–ceramic hydrogels and the freeze-drying pace (Pekor et al., 2008). The scaffolds were fabricated by the freeze-drying process to achieve extremely porous structures. Fig. 3 reveals the cross-sectional structures of hydrogels without and with crosslinkers (Fig. 3a and 3b) and the hydrogels containing 0.25, 1.0, and 1.5% SiC NPs (Fig. 3(c-e)). The uncrosslinked hydrogel has a porous structure with average pore sizes of about 290 μm (Fig. 3a). The addition of crosslinking agents reduced the pore sizes to be 235 μm (Fig. 3b). As indicated in Fig. 3(c-e), a highly interconnected and an almost uniform porous composition was observed by increasing the amount of SiC. The SEM images reveal that the hydrogels are greatly porous, and the average pores are in the range of 145–200 μm in size, which are essential for cartilage tissue

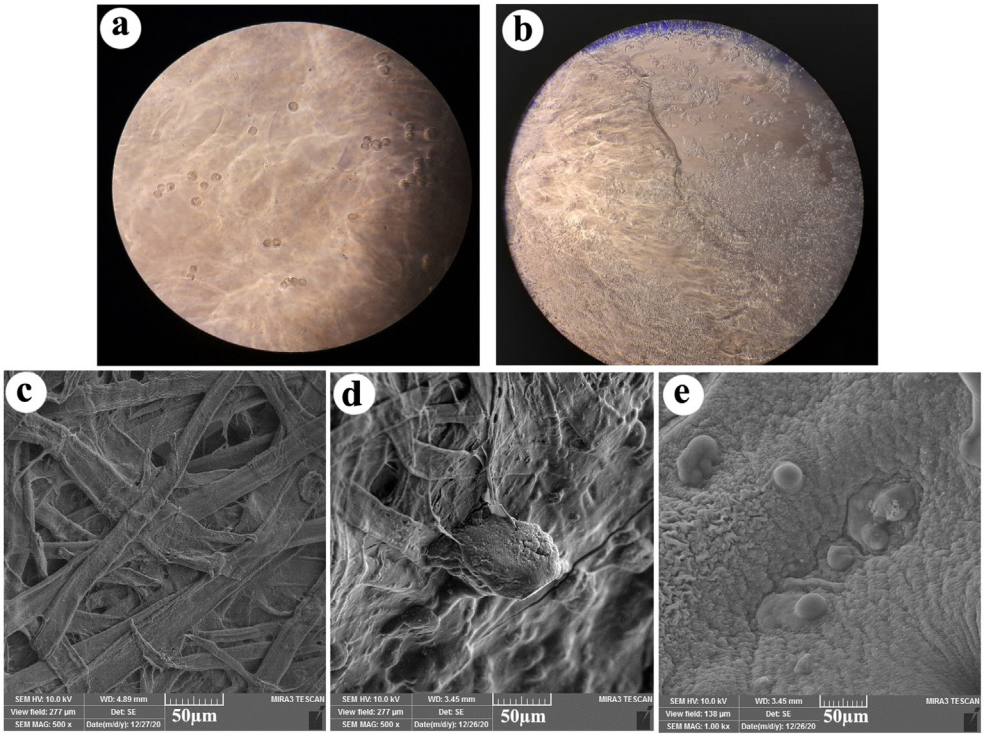

Fig. 6 Phase-contrast microscopy of hydrogel without SiC (a), and with 1.5% SiC (b), FESEM images of hydrogel without SiC (c), and with 1.5% SiC (d,e).

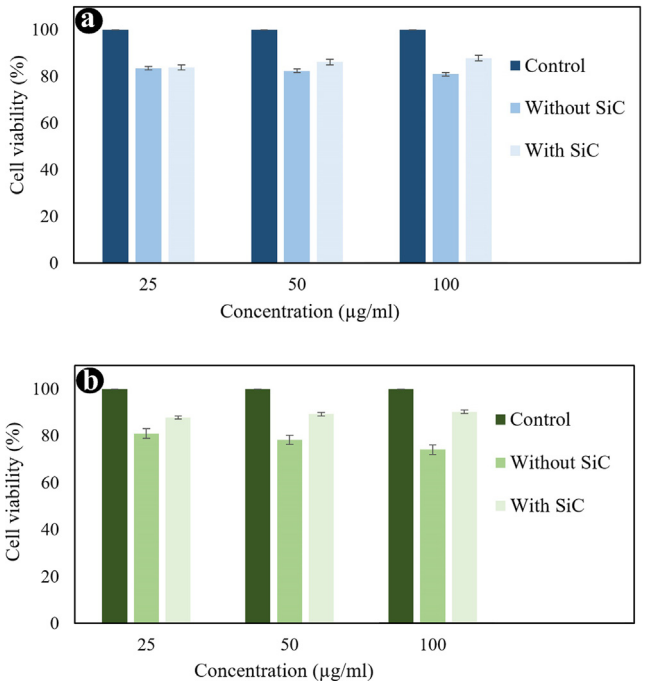

Fig. 7 Cell viability of hydrogels (a) after 24 h, and (b) 72 h incubation.

engineering (Zhu et al., 2009). Besides, the average of pores was reduced by increasing the SiC content.

Fig. 4 reveals the EDS spectra of as-prepared hydrogels. As can be seen, the spectrum of crosslinked hydrogel without SiC contains C, O, N, and Na elements. In addition to C, O, N elements, Si element exists in the hydrogels containing SiC, and by increasing the amount of SiC, the intensity of Si peaks are improved. Besides, a small amount of Au is observed in all hydrogels, which is related to the coating of the hydrogels with Au to conduct the samples

3.4. Swelling behavior

Swelling performance is a significant factor in cartilage tissue engineering. Ensuring the passage of nutrients through the scaffold is essential. The uptake ability of PBS defines the scaffold's water absorption capacity, which is an essential parameter that emphasizes the biological activity of the hydrogels. Fig. 5a unveils the swelling ratio of hydrogels after 24 h immersion in PBS at 37 °C. The highest swelling ratio was observed for crosslinked hydrogel without NPs (1060%) due to the large pore sizes, and the hydrogel containing 1.5% SiC NPs showed the lowest swelling ratio (714%) because of smaller pores. Loading SiC into hydrogel decreased the water uptake in the hydrogels (Xiao et al., 2012).

Fig. 5b reveals in vitro degradation of nanocomposite hydrogels over 21-day incubation in PBS buffer solution at 37 °C. In the first five days, all specimens showed an increase in mass, which may be due to swelling. The weight of all hydrogels incubated in PBS solution started to reduce continuously with time, and crosslinked hydrogel revealed the fastest and greatest mass loss between all hydrogels, which completely dissolved after 21 days. Therefore, the degradation rate of hydrogel with higher SiC content (1.5%) was slower than that of lower SiC content hydrogels. The lowest degradation was recognized for higher SiC content, which directly affected the total time needed to destroy the component (Kirchmajer et al., 2013).

3.5. Cell viability and adhesion

Nowadays it is clear that nanoparticles were shown to elicit cellular activities including cell differentiation, proliferation, and attachment in the transplanted tissue. In this investigation, SiC NPs embedded composite was applied to improve the cellular activities of the hydrogels. As indicated in both SEM and phase-contrast microscopy images, the potential ability of nanoparticles to increase cell adhesion is well observed (Fig. 6). Embedded SiC NPs supply a more efficient surface for cell adhesion than hydrogel without SiC. As presented in Fig. 7, the cell viability percentage of scaffolds was determined after 24 and 72 h of incubation. The cell viability was 87.90%, 86.26%, 83.92%, and which resultant in adding 100, 50, and 25 (μg/ml) of scaffold comprising 1.5% SiC NPs after 24 h, sequentially. Besides, the hydrogel without SiC exhibited 81.03%, 82.46%, and 83.59% cell viability after 24 h of incubation. The cell viability was 90.3%, 89.3%, and 87.9%, which is reached by adding 100, 50, and 25 (μg/ml) of the hydrogel comprising 1.5% SiC after 72 h incubation, sequentially. Moreover, the crosslinked scaffold (without SiC) unveiled 74.1%, 78.3%, and 81.0% cell viability after 72 h. Cell adhesion and proliferation significantly improved compared to crosslinked hydrogel without NPs (P-value < 0.05). Therefore, applying more NP concentration was effective to induce a significantly high level of live cells as compared with the blank (crosslinked hydrogel without NPs). OA/GEL composites embedded nanoparticles have showed excellent physical properties for tissue engineering in comparison with hydrogels without nanoparticles. Besides the improvement of physical properties, integrated SiC NPs into the hydrogel also improve cellular interaction, adhesion, viability, and differentiation which could impact the extracellular matrix deposition. Owning to the previous study, combining nanostructures in three-dimensional engineered tissues could decrease inflammation to transplanted tissues by the counterbalance of immune cell viability and cell adhesion (Divieto & Sassi, 2015). By comparing the results obtained for nanocomposites, it was confirmed that SiC NPs elicited the cell growth and viability (Hasan et al., 2018; Li et al., 2020; Smith et al., 2009).

4. Conclusion

Thermosensitive hydrogels with oxidized alginate, gelatin, and SiC NPs as injectable hydrogels have been successfully fabricated. The hydrogels show thermosensitive sol–gel properties with temperature gelation at 35 °C. The elasticity, G' and G'' improved by increasing the SiC NPs contents. In vitro degradation investigation proved that the degradation could be regulated by SiC modification. A primary in vitro cell culture research was carried out utilizing OA/GEL/SiC hydrogels as an injectable cell-carrier substance to trap L929 fibroblast cells. It was observed the hydrogels not only maintained the cell viability but also stimulate cell generation. These investigations designate that the thermosensitive OA/GEL/SiC hydrogels may possess excellent potential in cartilage tissue engineering purposes.

CRediT authorship contribution statement

Mojgan Ghanbari: Investigation, Formal analysis, Methodology, Writing – original draft, Software. **Masoud Salavati-Niasari:** Writing – review & editing, Conceptualization, Supervision, Project administration, Visualization, Data curation, Validation, Resources. **Fatemeh Mohandes:** Data curation, Validation, Resources. **Zohreh Firouzi:** Methodology.

Declaration of Competing Interest

The authors declare that they have no known competing financial interests or personal relationships that could have appeared to influence the work reported in this paper.

Acknowledgement

The authors thank the University of Kashan by Grant No (159271/09) and Iran National Science Foundation (INSF, 99017572; 97017837) for financing this investigation.

References

Afroz, S., Thomas, S. W., Mumcu, G., & Saddow, S. (2013). Implantable SiC based RF antenna biosensor for continuous glucose monitoring. SENSORS, 2013 IEEE,

Ahmed, E.M., 2015. Hydrogel: Preparation, characterization, and applications: A review. J. Adv. Res. 6 (2), 105–121. https://doi.org/10.1016/j.jare.2013.07.006.

Alsberg, E., Anderson, K.W., Albeiruti, A., Rowley, J.A., Mooney, D. J., 2002. Engineering growing tissues. Proc. Natl. Acad. Sci. 99 (19), 12025–12030.

Balakrishnan, B., Jayakrishnan, A., 2005. Self-cross-linking biopolymers as injectable in situ forming biodegradable scaffolds. Biomaterials 26 (18), 3941–3951.

Bang, S., Jung, U.-W., Noh, I., 2018. Synthesis and biocompatibility characterizations of in situ chondroitin sulfate–gelatin hydrogel for tissue engineering. Tissue Eng. Regenerative Med. 15 (1), 25–35.

Baniasadi, H., Mashayekhan, S., Fadaoddini, S., Haghirsharifzamini, Y., 2016. Design, fabrication and characterization of oxidized alginate–gelatin hydrogels for muscle tissue engineering applications. J. Biomater. Appl. 31 (1), 152–161. https://doi.org/10.1177/0885328216634057.

Bian, L., Zhai, D.Y., Tous, E., Rai, R., Mauck, R.L., Burdick, J.A., 2011. Enhanced MSC chondrogenesis following delivery of TGF-β3 from alginate microspheres within hyaluronic acid hydrogels in vitro and in vivo. Biomaterials 32 (27), 6425–6434.

Bock, P., Gierlinger, N., 2019. Infrared and Raman spectra of lignin substructures: Coniferyl alcohol, abietin, and coniferyl aldehyde. J. Raman Spectrosc. 50 (6), 778–792.

Bonaventura, G., Iemmolo, R., La Cognata, V., Zimbone, M., La Via, F., Fragalà, M.E., Barcellona, M.L., Pellitteri, R., Cavallaro, S., 2019. Biocompatibility between silicon or silicon carbide surface and neural stem cells. Sci. Rep. 9 (1), 1–13.

Boontheekul, T., Kong, H.-J., Mooney, D.J., 2005. Controlling alginate gel degradation utilizing partial oxidation and bimodal molecular weight distribution. Biomaterials 26 (15), 2455–2465.

Camarero-Espinosa, S., Rothen-Rutishauser, B., Weder, C., Foster, E. J., 2016. Directed cell growth in multi-zonal scaffolds for cartilage tissue engineering. Biomaterials 74, 42–52.

Chen, F., Ni, Y., Liu, B., Zhou, T., Yu, C., Su, Y., Zhu, X., Yu, X., Zhou, Y., 2017. Self-crosslinking and injectable hyaluronic acid/RGD-functionalized pectin hydrogel for cartilage tissue engineering. Carbohydr. Polym. 166, 31–44.

Chen, S., Zhang, Q., Nakamoto, T., Kawazoe, N., Chen, G., 2016. Gelatin scaffolds with controlled pore structure and mechanical property for cartilage tissue engineering. Tissue Eng. Part C: Methods 22 (3), 189–198.

Chiu, Y.-L., Chen, S.-C., Su, C.-J., Hsiao, C.-W., Chen, Y.-M., Chen, H.-L., Sung, H.-W., 2009. pH-triggered injectable hydrogels prepared from aqueous N-palmitoyl chitosan: In vitro characteristics and in vivo biocompatibility. Biomaterials 30 (28), 4877–4888. https://doi.org/10.1016/j.biomaterials.2009.05.052.

Choi, H.S., Huh, K.M., Ooya, T., Yui, N., 2003. pH- and Thermosensitive Supramolecular Assembling System: Rapidly Responsive Properties of β-Cyclodextrin-Conjugated Poly(ε-lysine). J. Am. Chem. Soc. 125 (21), 6350–6351. https://doi.org/10.1021/ja034149x.

Divieto, C., Sassi, M.P., 2015. A first approach to evaluate the cell dose in highly porous scaffolds by using a nondestructive metabolic method. Future Sci. OA 1 (4).

Emami, Z., Ehsani, M., Zandi, M., Foudazi, R., 2018. Controlling alginate oxidation conditions for making alginate-gelatin hydrogels. Carbohydr. Polym. 198, 509–517.

Epstein-Barash, H., Stefanescu, C.F., Kohane, D.S., 2012. An in situ cross-linking hybrid hydrogel for controlled release of proteins. Acta Biomater. 8 (5), 1703–1709. https://doi.org/10.1016/j.actbio.2012.01.028.

Frewin, C. L., Saddow, S. E., & Coletti, C. (2014). Graphene electrodes on a planar cubic silicon carbide (3C-SiC) long term implantable neuronal prosthetic device. In: Google Patents.

Han, L., Xu, J., Lu, X., Gan, D., Wang, Z., Wang, K., Zhang, H., Yuan, H., Weng, J., 2017. Biohybrid methacrylated gelatin/polyacrylamide hydrogels for cartilage repair. J. Mater. Chem. B 5 (4), 731–741.

Hasan, A., Morshed, M., Memic, A., Hassan, S., Webster, T.J., Marei, H.-E.-S., 2018. Nanoparticles in tissue engineering: applications, challenges and prospects. Int. J. Nanomed. 13, 5637.

Hiemstra, C., Zhou, W., Zhong, Z., Wouters, M., Feijen, J., 2007. Rapidly in Situ Forming Biodegradable Robust Hydrogels by Combining Stereocomplexation and Photopolymerization. J. Am. Chem. Soc. 129 (32), 9918–9926. https://doi.org/10.1021/ja072113p.

Hunt, J.A., Chen, R., van Veen, T., Bryan, N., 2014. Hydrogels for tissue engineering and regenerative medicine [10.1039/C4TB00775A]. J. Mater. Chem. B 2 (33), 5319–5338. https://doi.org/10.1039/C4TB00775A.

Ikada, Y., 2006. Challenges in tissue engineering. J. R. Soc. Interface 3 (10), 589–601.

Jejurikar, A., Seow, X.T., Lawrie, G., Martin, D., Jayakrishnan, A., Grøndahl, L., 2012. Degradable alginate hydrogels crosslinked by the macromolecular crosslinker alginate dialdehyde [10.1039/C2JM30564J]. J. Mater. Chem. 22 (19), 9751–9758. https://doi.org/10.1039/C2JM30564J.

Jin, R., Teixeira, L.M., Dijkstra, P.J., Karperien, M., Van Blitterswijk, C., Zhong, Z., Feijen, J., 2009. Injectable chitosan-based hydrogels for cartilage tissue engineering. Biomaterials 30 (13), 2544–2551.

Kimura, Y., Ozeki, M., Inamoto, T., Tabata, Y., 2003. Adipose tissue engineering based on human preadipocytes combined with gelatin microspheres containing basic fibroblast growth factor. Biomaterials 24 (14), 2513–2521.

Kirchmajer, D.M., Watson, C.A., Ranson, M., 2013. Gelapin, a degradable genipin cross-linked gelatin hydrogel. RSC Adv. 3 (4), 1073–1081.

Kreeger, P.K., Woodruff, T.K., Shea, L.D., 2003. Murine granulosa cell morphology and function are regulated by a synthetic Arg–Gly–Asp matrix. Mol. Cell. Endocrinol. 205 (1–2), 1–10.

Kuzmanović, M., Božanić, D.K., Milivojević, D., Ćulafić, D.M., Stanković, S., Ballesteros, C., Gonzalez-Benito, J., 2017. Sodium-alginate biopolymer as a template for the synthesis of nontoxic red emitting Mn 2+-doped CdS nanoparticles. RSC Adv. 7 (84), 53422–53432.

Li, H., Pan, S., Xia, P., Chang, Y., Fu, C., Kong, W., Yu, Z., Wang, K., Yang, X., Qi, Z., 2020. Advances in the application of gold nanoparticles in bone tissue engineering. J. Biol. Eng. 14, 1–15.

Li, L., Yan, B., Yang, J., Chen, L., Zeng, H., 2015. Novel Mussel-Inspired Injectable Self-Healing Hydrogel with Anti-Biofouling Property. Adv. Mater. 27 (7), 1294–1299. https://doi.org/10.1002/adma.201405166.

Li, X., Xu, A., Xie, H., Yu, W., Xie, W., Ma, X., 2010. Preparation of low molecular weight alginate by hydrogen peroxide depolymerization for tissue engineering. Carbohydr. Polym. 79 (3), 660–664.

Macaya, D., Ng, K.K., Spector, M., 2011. Injectable collagen–genipin gel for the treatment of spinal cord injury: in vitro studies. Adv. Funct. Mater. 21 (24), 4788–4797.

Morouço, P., Fernandes, C., & Santos-Rocha, R., 2019. Osteoarthritis, Exercise, and Tissue Engineering: A Stimulating Triad for Health Professionals. J. Aging Res., 2019.

Nezhad-Mokhtari, P., Ghorbani, M., Roshangar, L., Rad, J.S., 2019. Chemical gelling of hydrogels-based biological macromolecules for tissue engineering: Photo-and enzymatic-crosslinking methods. Int. J. Biol. Macromol. 139, 760–772.

Nguyen, T.-P., Lee, B.-T., 2011. Fabrication of oxidized alginate-gelatin-BCP hydrogels and evaluation of the microstructure, material properties and biocompatibility for bone tissue regeneration. J. Biomater. Appl. 27 (3), 311–321. https://doi.org/10.1177/0885328211404265.

Oliveros, A., Guiseppi-Elie, A., Saddow, S.E., 2013. Silicon carbide: a versatile material for biosensor applications. Biomed. Microdevices 15 (2), 353–368.

Park, H., Lee, H.J., An, H., Lee, K.Y., 2017. Alginate hydrogels modified with low molecular weight hyaluronate for cartilage regeneration. Carbohydr. Polym. 162, 100–107.

Pawde, S.M., Deshmukh, K., 2008. Characterization of polyvinyl alcohol/gelatin blend hydrogel films for biomedical applications. J. Appl. Polym. Sci. 109 (5), 3431–3437. https://doi.org/10.1002/app.28454.

Pekor, C.M., Kisa, P., Nettleship, I., 2008. Effect of Polyethylene Glycol on the Microstructure of Freeze-Cast Alumina. J. Am. Ceram. Soc. 91 (10), 3185–3190.

Rogalsky, A.D., Kwon, H.J., Lee-Sullivan, P., 2011. Compressive stress–strain response of covalently crosslinked oxidized-alginate/N-succinyl-chitosan hydrogels. J. Biomed. Mater. Res. Part A 99 (3), 367–375.

Saddow, S.E., 2012. Silicon carbide biotechnology: a biocompatible semiconductor for advanced biomedical devices and applications. Elsevier.

Sarker, B., Papageorgiou, D.G., Silva, R., Zehnder, T., Gul-E-Noor, F., Bertmer, M., Kaschta, J., Chrissafis, K., Detsch, R., Boccaccini, A.R., 2014. Fabrication of alginate–gelatin crosslinked hydrogel microcapsules and evaluation of the microstructure and physicochemical properties. J. Mater. Chem. B 2 (11), 1470–1482.

Smith, I., Liu, X., Smith, L., Ma, P., 2009. Nanostructured polymer scaffolds for tissue engineering and regenerative medicine. Wiley Interdiscip. Rev. Nanomed. Nanobiotechnol. 1 (2), 226–236.

Tan, R., Feng, Q., She, Z., Wang, M., Jin, H., Li, J., Yu, X., 2010. In vitro and in vivo degradation of an injectable bone repair composite. Polym. Degrad. Stab. 95 (9), 1736–1742.

Tengroth, C., Gasslander, U., Andersson, F.O., Jacobsson, S.P., 2005. Cross-linking of gelatin capsules with formaldehyde and other aldehydes: an FTIR spectroscopy study. Pharm. Dev. Technol. 10 (3), 405–412.

Tønnesen, H.H., Karlsen, J., 2002. Alginate in drug delivery systems. Drug Dev. Ind. Pharm. 28 (6), 621–630.

Van Vlierberghe, S., Dubruel, P., Schacht, E., 2011. Biopolymer-based hydrogels as scaffolds for tissue engineering applications: a review. Biomacromolecules 12 (5), 1387–1408.

Vieira, E.F.S., Cestari, A.R., Airoldi, C., Loh, W., 2008. Polysaccharide-Based Hydrogels: Preparation, Characterization, and Drug Interaction Behaviour. Biomacromolecules 9 (4), 1195–1199. https://doi.org/10.1021/bm7011983.

Vinatier, C., Bouffi, C., Merceron, C., Gordeladze, J., Brondello, J.-M., Jorgensen, C., Weiss, P., Guicheux, J., Noel, D., 2009. Cartilage Tissue Engineering: Towards a Biomaterial-Assisted Mesenchymal Stem Cell Therapy. Curr. Stem Cell Res. Ther. 4 (4), 318–329. https://doi.org/10.2174/157488809789649205.

Vinatier, C., Guicheux, J., 2016. Cartilage tissue engineering: From biomaterials and stem cells to osteoarthritis treatments. Ann. Phys. Rehabilit. Med. 59 (3), 139–144. https://doi.org/10.1016/j.rehab.2016.03.002.

Xiao, W., Liu, W., Sun, J., Dan, X., Wei, D., Fan, H., 2012. Ultrasonication and Genipin Cross-Linking to Prepare Novel Silk Fibroin-Gelatin Composite Hydrogel. J. Bioactive Compatible Polym. 27 (4), 327–341. https://doi.org/10.1177/0883911512448692.

Xing, Q., Yates, K., Vogt, C., Qian, Z., Frost, M.C., Zhao, F., 2014. Increasing mechanical strength of gelatin hydrogels by divalent metal ion removal. Sci. Rep. 4, 4706.

Xu, J., Liu, Y., Hsu, S.-H., 2019a. Hydrogels based on Schiff base linkages for biomedical applications. Molecules 24 (16), 3005.

Xu, Y., Peng, J., Richards, G., Lu, S., Eglin, D., 2019b. Optimization of electrospray fabrication of stem cell–embedded alginate–gelatin microspheres and their assembly in 3D-printed poly (ε-caprolactone) scaffold for cartilage tissue engineering. J. Orthopaedic Trans. 18, 128–141.

Yang, J.-S., Xie, Y.-J., He, W., 2011. Research progress on chemical modification of alginate: A review. Carbohydr. Polym. 84 (1), 33–39.

Zhu, W., Xiao, J., Wang, D., Liu, J., Xiong, J., Liu, L., Zhang, X., Zeng, Y., 2009. Experimental study of nano-HA artificial bone with different pore sizes for repairing the radial defect. Int. Orthop. 33 (2), 567–571.